JOURNAL OF OPTOELECTRONICS AND ADVANCED MATERIALS Vol. 17, No. 7-8, July – August 2015, p. 1122 - 1127

A structural model for scattering intensities with multiple fractal regions

E. M. ANITAS[a, b]
[a]*Joint Institute for Nuclear Research, 141980 Dubna, Moscow region, Russian Federation*
[b]*Horia Hulubei National Institute of Physics and Nuclear Engineering, RO-077125 Bucharest-Magurele, Romania*

We report here a new structural model based on deterministic fat fractals (fractals with positive Lebesgue measure) which describes experimental small-angle scattering (SAS) data characterized by a succesion of fractal regions with arbitrarily lengths. We calculate analytically the corresponding mono- and polydisperse structure factors. We study its properties in momentum space and show how one can extract the upper and lower edges of the fractals and the crossover position between fractal regions with different scattering exponents. The latter quantities are correlated to the variation of scaling factor with the iteration number, and can be used to estimate the sizes of fractal subunits. In order to illustrate the applicability of the obtained results to various nano- and microstructures, we study the scattering properties of the fattened version of two well-known regular $3D$ fractals: Cantor sets and Menger sponge.

(Received May 7, 2015; accepted June 24, 2015)

Keywords: Small-angle scattering, Fractals, Structural properties

1. Introduction

The small-angle scattering (SAS) technique (neutrons, X-ray, light) is one of the most important investigation method of structural properties of disordered matter at nano- and microscales, since it's non-destructive and the obtained quantities are averaged over a macroscopic volume [1 - 3]. It yields the elastic cross section per unit solid angle as a function of momentum transfer, which describes, through a Fourier transform, the spatial density-density correlations in the irradiated sample. The measured physical quantity in a SAS experiment is the normalized cross section per unit volume (scattering intensity), which is defined by $I(q) \equiv (1/V')d\sigma/d\Omega$, where $q = 4\pi/\lambda \sin\theta$, λ is the wavelength of the incident radiation, and θ is half the scattering angle.

Many disordered nano- and microsystems, such as elastomeric membranes [4, 5], cement [6], magnetic [7, 8], or biological structures [9 - 11] have the self-similarity property in a certain scale, and this may play an important role on electromagnetic [12], statistical [13], electrical [14] or optical [15] properties. Therefore, the concept of fractal geometry [16, 17] together with SAS technique can be used to obtain new insights about the structural properties of such systems [18].

For random (statistical self-similar) fractals, the main parameters which can be obtained is the fractal dimension of the system and the lower and upper edge of the fractal regions. Thus, the main advantage in using SAS for investigating fractal structures resides in its abillity to differentiate between mass and surface fractals [19, 20], through the value of power-law scattering exponent of the simple power-law decay $I(q) \propto q^{-\tau}$, where $\tau = D_m$ for mass fractals, and $\tau = 6 - D_s$, for surface fractals. Here D_m, with $0 < D_m < 2$ is the mass fractal dimension, and D_s, with $2 < D_s < 3$ is the surface fractal dimension.

For regular deterministic (exact self-similar) mass fractals, the monodisperse SAS intensity shows a superposition of maxima and minima on a simple power-law decay [21 - 25] and, therefore, additional information can be extracted, such as the scaling factor β_s (from the period in the double logarthmic scale), the number of fractal iteration (from the number of periods of the function $I(q)q^{-D_m}$), and the total number N_m of structural subunits of which the fractal is composed (from the relation $N_m = (1/\beta_s)^{m\,D_m}$) [23, 25]. By extending such deterministic models to multi-phase fractal systems one can reveal wether one fractal „absorbs" into another one, or they are both immersed in a surrounding medium [26]. In the case of deterministic fractals having iteration-dependent scaling factors, the structural characteristics *at each level* can be obtained, as well [27].

For single power-law decays, as well as for multiple power-law decays of fixed length (and at a given scaling factor) the information concerning the sizes of the fractals and of its subunits can be extracted (within the limits of the experimental setup), from the beggining (and, respectively the end) of the fractal region, and from the position of the crossover between the power-law decays with different scattering exponents [25 - 28]. However, for a *succesion* of several power-law decays, the length of each individual decay can take arbitrarily values, and a theoretical model, which properly can take into account this feature, has not yet been developed.

In this work, we address this issue and a new structural model with iteration-dependent scaling factors is developed. We perform numerical calculations of the scattering structure factor on a system of randomly

oriented and uniformly distributed $3D$ fractals. We show that, for a given scaling factor, the length of the fractal regions can be obtained by a generalization of the function generating the subsequent fractal scaling factors. We confirm our results by considering two basic models based on the fattened versions of Cantor set and, respectively Menger sponge, containing cubes as basic units.

2. Theoretical background

We consider a two-phase system consisting of microscopic fractal objects with scattering length b_j and scattering length density (SLD) ρ_m, immersed into a solid matrix of SLD ρ_p. If V' is the irradiated volume by the incident beam (neutrons, X-ray, light), the cross section can be written as $d\sigma/d\Omega = |A(\vec{q})|^2$, with $A(\vec{q}) \equiv \int_{V'} \rho_s(\vec{r}')e^{-i\vec{q}.\vec{r}}d^3\vec{r}$, $\rho_s(\vec{r}) = \sum_j b_j\delta(\vec{r} - \vec{r}_j)$, and $\vec{r}_j$ are the objects positions. Then, the scattering intensity becomes

$$I(q) = n|\Delta\rho|^2V^2\langle|F(\vec{q})|^2\rangle, \quad (1)$$

where n is the fractal concentration, V is the volume of the fractal object, $\Delta\rho \equiv \rho_m - \rho_p$ is the scattering contrast, $F(\vec{q}) = (1/V)\int_V e^{-i\vec{q}.\vec{r}}d\vec{r}$ with $F(0) = 1$ is the normalized form factor, and $\langle \dots \rangle$ represents the ensemble averaging over all orientations of the objects. We consider that the probability of any orientation is the same and therefore the ensemble averaging can be obtained by integrating over the solid angle in spherical coordinates. Thus, one obtains $\langle f(q_x, q_y, q_z)\rangle \equiv 1/(4\pi)\int_0^\pi d\theta \sin\theta \int_0^{2\pi} d\phi f(q, \theta, \phi)$, with $q_x = a\cos\phi\sin\theta$, $q_y = q\sin\phi\sin\theta$, $q_z = q\cos\theta$.

For a deterministic fractal with balls of radius R as subunits, the scattering intensity is [25]

$$I(q) = \frac{I(0)S(q)|F_0(\vec{q}R)|^2}{N_m}, \quad (2)$$

where $I(0) = n|\Delta\rho|^2V^2$ is the intensity at zero angle, $F_0(\vec{q}R)$ is the form factor of the fractal subunits (balls, in Eq. (2)), N_m is the number of fractal subunits, and

$$S(q) \equiv \frac{\langle\rho_{\vec{q}}\rho_{-\vec{q}}\rangle}{N_m}, \quad (3)$$

with $\rho_{\vec{q}} = \sum_j e^{-i\,\vec{q}.\vec{r}_j}$, beying the Fourier transform of the density of ball centers.

The polydispersity is taken into account by considering a log-normal distribution $D_N(l)$ of the scatterer size [25], where the mean length l_0 and its relative variance σ_r are given by

$$\mu_0 \equiv \langle l\rangle_D, \quad \sigma_r \equiv \frac{(\langle l^2\rangle_D - \mu_0^2)^{\frac{1}{2}}}{\mu_0}. \quad (4)$$

3. Construction of fat fractals

The construction of the Cantor set and Menger sponge is very similar to that of generalized regular mass Cantor and Vicsek fractals [23, 25]. In both cases we apply a top-down approach in which an initial structure (here cube, but any other shape could be used as well) of edge length l_0 is repeatedly divided into smaller cubes, according to a given rule (see below).

In order to obtain a deterministic fractal we proceed as follows: one consider the initial cube (initiator) as the $m = 0$-th iteration. Then, this is divided into 27 smaller cubes with side length $1/3$ from the initiator. The next iteration ($m = 1$) implies that some cubes (out of 27 ones) are kept and others are removed, and depending on how many are kept and at which positions, it defines the generator of the fractal. In particular, for Cantor sets we keep the 8 cubes from the corners and remove all the others, while for the Menger sponge we remove the smaller cubes in the middle of each face together with the cube in the center, and keep all the others. By repeating the same operation on each of the remaining cubes (8 for Cantor set, 20 for Menger sponge), one obtains (at $m = 2$) 64, and respectively 400 cubes of side length $1/3^2$ from the initiator. Therefore, the cubes at m-th iteration have the side length $l_m = (1/3)^m l_0$, and their number is given by

$$N_m = \begin{cases} 8^m, & for\ Cantor\ set \\ 20^m, & for\ Menger\ sponge \end{cases}. \quad (5)$$

By considering the limit $m \to \infty$, the regular (thin; and which corresponds to the scaling factor $1/3$ in the generalized Cantor fractal [23]) Cantor set and Menger sponge have an iteration-independent fractal dimensios $\log 8/\log 3 = 1.89$ and respectively $\log 20/\log 3 = 2.73$. The "fattened" version of the above fractals is obtained by keeping the side length $1/3$ for first m_1 (> 1) iterations, then keeping the side length $1/3^2$ for next m_2 (> 1) iterations etc. The final structure is topologically equivalent to the regular structure, but the "holes" decrease in size sufficiently fast, so that for $m \to \infty$, the fractal has nonzero and finite volume (hence, the name *fat* fractal).

Here, the construction process is very similar to that described in Ref. [27]: we specify the initiator in Cartesian coordinates as a set satisfying the inequalities $-l_0/2 \le x_i \le l_0/2$, where $i = 1, 2, 3$, and x_i are the three directions. The origin lies in the center of initiator, and the axes are parallel to its edges. The iteration rule ($m = 1$, generator) is to replace the initiator by cubes of edge length $\beta_s^{(1)}l_0$. Note, that whenever the quantity $(\dots)$ appears in the exponent, it is to be interpreted as an index and not a power. For the Cantor set, the centers of the 8 cubes are shifted from the origin by the vectors $\vec{a}_j = \{\pm\beta_t^{(1)}l_0, \pm\beta_t^{(1)}l_0, \pm\beta_t^{(1)}l_0\}$ with all the combinations of the signs, where $\beta_t^{(1)} \equiv (1 - \beta_s^{(1)})/2$. For the Menger sponge we have, as in the case of Cantor set, 8 cubes shifted by $\vec{a}_j$, but with 12 additional cubes shifted by $\left\{\pm\beta_t^{(1)}l_0, \pm\beta_t^{(1)}l_0, 0\right\}$, $\left\{\pm\beta_t^{(1)}l_0, 0, \pm\beta_t^{(1)}l_0\right\}$ and

$\left\{0, \pm\beta_t^{(1)} l_0, \pm\beta_t^{(1)} l_0\right\}$. The next $m_1 - 1$ iterations are obtained by the same procedure and with the same values of $\beta_s^{(1)}$. However, for the next m_2 iterations we consider $\beta_s^{(2)}$, for next m_3 iterations we take $\beta_s^{(3)}$ and so on (Fig. 1). Thus, for "fattened" versions the edge of the removed parallelepiped at m-th iteration is $\gamma_m = \alpha^{p_m}$, where $0 < \alpha < 1$ and

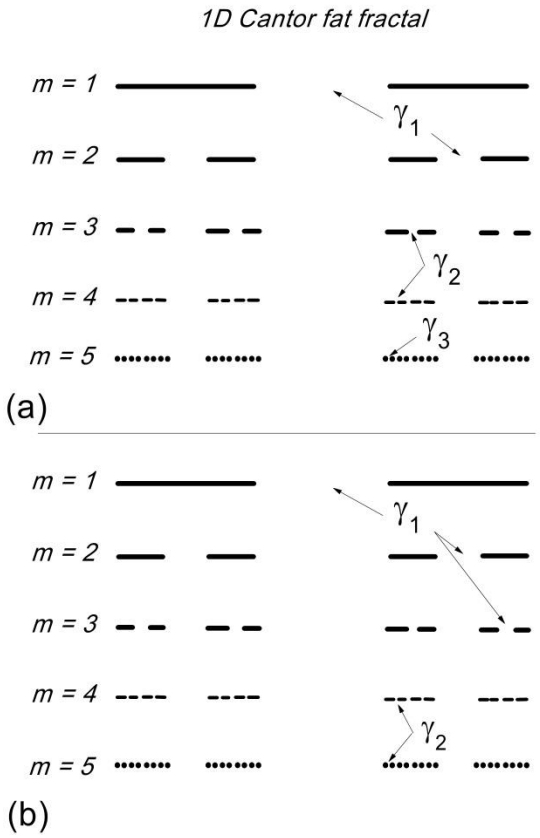

Fig. 1. Construction of the one-dimensional Cantor fat fractal for various values of the number of iterations at which the scaling factors are kept constant. (a)$m_1 = 2, m_2 = 2, m_3 = 2, \ldots$; (b) $m_1 = 3, m_2 = 3, m_3 = 3, \ldots$.

$$p_m = \begin{cases} 1, & m = 1, \ldots, m_1 \\ 2, & m = m_1, \ldots\ m_1 + m_2 \\ \ldots\ \ldots\ \ldots\ \ldots\ \ldots\ \ldots\ \ldots\ \ldots\ \ldots\ \ldots \end{cases}. \quad (6)$$

Thus, the edge length of each remained cube is $l_m = l_0/2^m \prod_{i=1}^{m}(1-\gamma_i)$, the scaling factor at m-th iteration is

$$\beta_s^{(m)} = \frac{1-\gamma_m}{2}, \quad (7)$$

and

$$\beta_t^{(m)} = \frac{l_{m-1}(1+\gamma_m)}{4}, \quad (8)$$

Depending on the particular values of $m_i, i = 1, \ldots, k$ one can generate fractal structures built from a succession of exact self-similar fractals, the former ones having different scaling factors at different scales (Fig. 2). By taking into account that $D_m = -3\log 2 / \log \beta_s^{(m)}$, we shall expect a succession of power-law decays of the form $S(q) \propto q^{-D_m}$ [27] but with fractal regions of arbitrarily length.

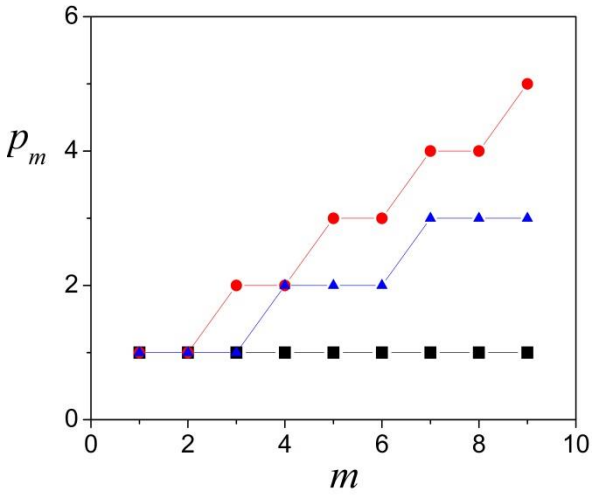

Fig. 2. (Color online) Variation of function p_m (Eq. (6); and implicitly of the values of the scaling factor) with the iteration number m. Black (squares): one scaling factors for all iterations (which is a regular deterministic fractal); Red (disks): one scaling factor starting with every second iteration; Blue (triangles): one scaling factor starting with every third iteration.

4. Results and discussions

The positions of the cube centers of Cantor set and Menger sponge can be written through their generative function as [23]

$$G_i^{(CS)}(\vec{q}) = \cos(q_x u_i)\cos\left(q_y u_i\right)\cos(q_z u_i), \quad (9)$$

and, respectively

$$G_i^{(MS)}(\vec{q}) = \frac{1}{20}\Big(G_i^{(CS)}(\vec{q}) + 4\left(L_i^{xz}(\vec{q}) + L_i^{xy}(\vec{q}) + L_i^{yz}(\vec{q})\right)\Big), \quad (10)$$

where we write $L_i^{xz}(\vec{q}) = \cos(q_x u_i)\cos(q_z u_i)$, $L_i^{xz}(\vec{q}) = \cos(q_x u_i)\cos(q_z u_i)$, $L_i^{yz}(\vec{q}) = \cos\left(q_y u_i\right)\cos(q_z u_i)$ and $u_i = l_0 \beta_t^{(i)} \prod_{j=1}^{i-1} \beta_s^{(j)}$. Therefore, the fractal structure factor [3] becomes

$$S(q) = N_m \begin{cases} \langle \left|G_i^{(CS)}(\vec{q})\right|^2 \rangle, & for\ Cantor\ set \\ \langle \left|G_i^{(MS)}(\vec{q})\right|^2 \rangle, & for\ Menger\ sponge. \end{cases} \quad (11)$$

The results for the monodisperse fat fractals are shown in Fig. 3 where we can see that the structure factor is characterized by three main regions: at low q ($\lesssim 4$ Å^{-1}) we have a plateau on a double logarithmic scale, and this gives the radius of gyration of the overall fractal, and finally an estimation of its upper edge. Analytical solutions for various fractals have been recently developed [23, 25, 27]. At intermediate q ($4 \div 1000$ Å^{-1} for $m = 4$, and $4 \div 20000$ Å^{-1} for $m = 6$) we have a succession of minima and maxima on a simple power-law decay with various values of scattering exponents. The length of each power-law decay increases with increasing the number of iterations for which we keep fixed the scaling factor. The crossover position (region where the scattering exponents change) between the fractal regions is situated after the last iteration with scaling factor $\beta_s^{(1)}$ and before first iteration with scaling factor $\beta_s^{(2)}$.

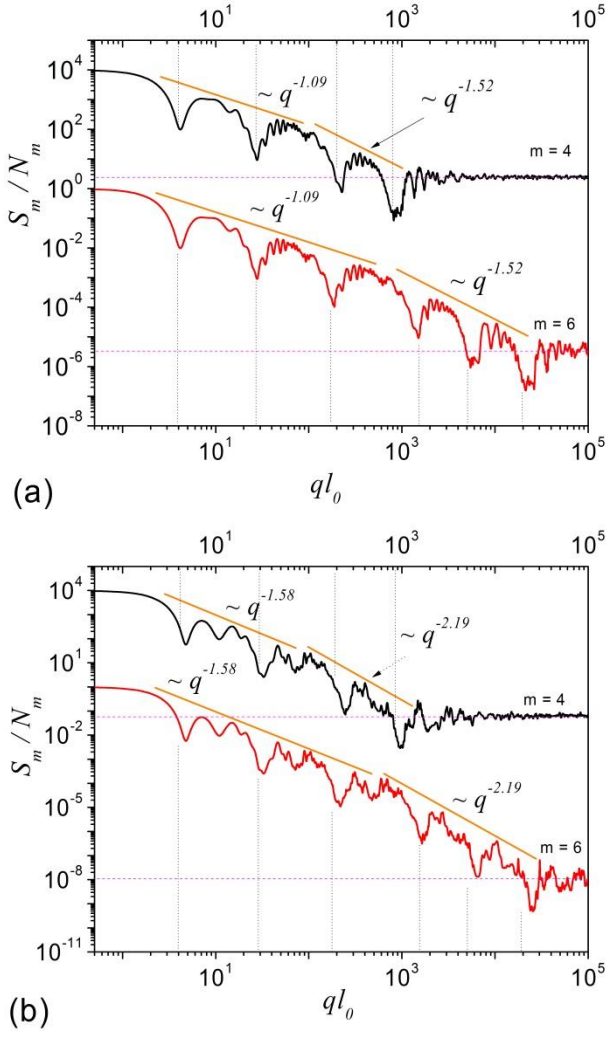

Fig. 3. (Color online) Monodisperse fractal structure factor (Eq. (11)) for: (a) Cantor set; (b) Menger sponge. The black (upper) curves ($m_1 = m_2 = 2$) are shifted vertically by a factor of 10^4 with respect to red (lower) curves ($m_1 = m_2 = 3$) in order to increase readability. The vertical lines are the minima positions (Eq. (12)). The horizontal lines are the asymptotes, given by $1/N_m$.

For both structures, the position of minima is reached when the fractal subunits interfere out of phase, and thus for m-th iteration we have

$$q_k l_0 \approx \frac{\pi}{2\beta_t^{(k)} \prod_{i=1}^{k} \beta_s^{(i)}}, \tag{12}$$

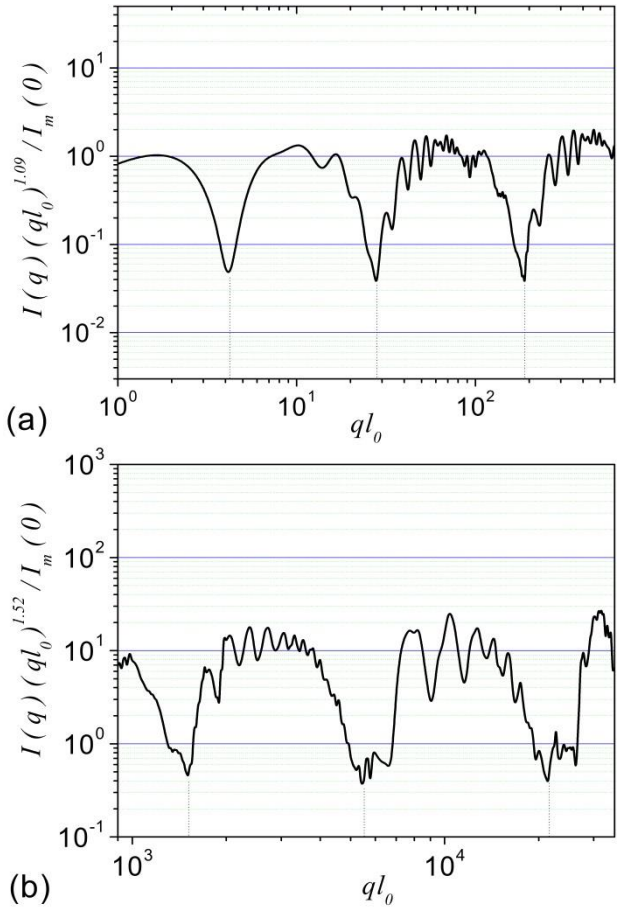

Fig. 4. (Color online) The log-periodicity of $I(q)q^{D_m}$ for the fat Cantor set. The periods are related to the scaling factor. The number of minima equals the iteration number of constant scaling factor. (a) $m_1 = m_2 = 2$; (b) $m_1 = m_2 = 3$.

Minima positions are marked by vertical lines in Figs. 3 and 4, and they show a good agreement with Eq. (12). The asymptote (the region beyond the last power-law decay) of the structure factor is $1/N_m$, and coincides with the asymptote of the regular fractals, since in this region $S(q) \cong 1$ [23, 25] and the number of particles (at a given iteration and generative function) is the same for both, regular and fat fractals. The region between the end of the intermediate region, and the beginning of the asymptotic region gives information about the size of smallest subunit of the fractal and thus about the lower edge of the fractal. [23, 25].

Important features of the fractals can be obtained from a graph of $I(q)q^{D_m}$ $vs.$ q on a double logarithmic scale

[25], for each fractal regions of the scattering intensity. Thus, the log-period is equal to $\log_{10}(1/\beta_s^{(1)})$ for the first fractal region, and is equal to $\log_{10}(1/\beta_s^{(2)})$ for the second fractal region. The number of minima in a given region is equal with the number of iterations at a constant value of the scaling factor. Fig. 4 shows the log-periodicity of fat Cantor set at $m_1 = m_2 = 2$ and $m_1 = m_2 = 3$ for both fractal regions ($I(q)q^{1.09}\ vs.\ q$ in Fig. 4a, and $I(q)q^{1.52}\ vs.\ q$ in Fig. 4b), where the scaling scaling factors and the number of minima are clearly revealed at various scales (spatial regions of constant scaling factors).

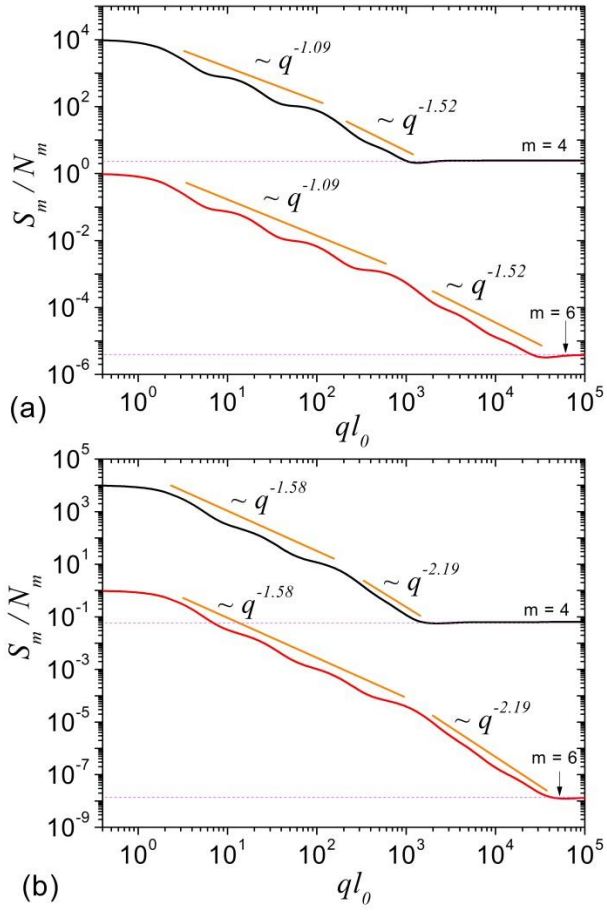

Fig. 5. (Color online) Polydisperse fractal structure factor with relative variance $\sigma_r = 0.5$ for: (a) Cantor set; (b) Menger sponge. The black (upper) curves ($m_1 = m_2 = 2$,) are shifted vertically by a factor of 10^4 with respect to red (lower) curves ($m_1 = m_2 = 3$) in order to increase readability. The horizontal lines are the asymptotes, given by $1/N_m$.

The effects of polydispersity are shown in Fig. 5, where we can see the succession of simple power-law decays with decreasing values of the scattering exponents. The curves becomes smoother (as compared with monodisperse case, see Fig. 3) and the power-law scattering exponents, the relative lengths of the fractal regions together with the values of the asymptotes are preserved. This shows that by taking into account the polydispersity, we can apply the developed model to a large class of experimental SAS data.

5. Conclusions

We have developed a theoretical model that generalizes the well-known mass fat fractals. We calculated analytically the corresponding mono- and polydisperse structure factor from a system of $3D$ Cantor set, and respectively Menger sponge, and have shown how one can extract the structural information.

The model can be applied to experimental data which shows a succession of fractal power-law (generalized or simple) decays with arbitrarly decreasing values of the scattering exponents. We have emphasized its main feature to describe the individual power-lw decays with variable length. It has been shown that the length of each power-law decay is correlated with the number of iterations fow which one keeps constant the scaling factor.

The proposed model is aimed at describing microstructural properties of various hierarchical structures (nano- and/or microclusters, biological objects, advanced artificially created micromaterials etc.), and it can be easily extended to take into account various relative positions and shapes of the fractal subunits, as well as various types of polydispersity.

Acknowledgments

The author is grateful to A. Yu. Cherny, V. A. Osipov and A. I. Kuklin for valuable discussions, and acknowledge the support from the grants/projects of the Romanian Governmental Representative at JINR.

References

[1] O. Glatter, O. Kratky, Small-Angle X-ray Scattering, Academic Press, London, 1982.
[2] L. A. Feigin, D. I. Svergun, Structure Analysis by Small-Angle X-Ray and Neutron Scattering, New-York: Plenum Press, 1987.
[3] P. Lindner, Th. Zemb, Neutron, X-Rays and Light Scattering: Scattering Methods Applied to Soft Condensed Matter, North-Holland, 2002.
[4] M. Balasoiu, E. M. Anitas, I. Bica, R. Erhan, V. A. Osipov, O. L. Orelovich, D. Savu, S. Savu, A. I. Kuklin, Optoelectron. Adv. Mater.-Rapid Commun. **2**, 730 (2008).
[5] E. M. Anitas, M. Balasoiu, I. Bica, V. A. Osipov, A.I. Kuklin, Optoelectron. Adv. Mater.-Rapid Commun. **3**, 621 (2009).
[6] A. Das, S. Mazumder, D. Sen, V. Yalmali, J. G. Shah, A. Ghosh, A. K. Sahu, P. K. Wattal - J. Appl. Cryst. **47**, 421 (2014).
[7] K. Cho, P. Biswas, P. Fraundorf - J. Ind. Eng. Chem. **20**, 558 (2014).

[8] M. L. Craus, A. K. Islamov, E. M. Anitas, N. Cornei, D. Luca, Journal of Alloys and Compounds **592**, 121 (2014).
[9] T. Naito, H. Yamamoto, K. Okuda, K. Konishi, H. Mayama, D. Yamaguchi, S. Koizumi, K. Kubo, T. Nakamura - Eur. Phys. J. B **86**, 410 (2014).
[10] I. Yadav, S. Kumar, V. K. Aswal, J. Kohlbrecher - Phys. Rev. E **89**, 032304 (2014).
[11] R. Gebhardt - J. Appl. Cryst. **47**, 29 (2014).
[12] X. Huang, S. Xiao, L. Zhou, C. T. Chan, P. Sheng, "Metamaterials: Theory, Design, and Applications", Springer, New York, (2009), Chap. 10, pp. 215–245.
[13] J. H. Luscombe, R. C. Desai, Phys. Rev. B, **32**, 1614 (1985).
[14] I. Bica, E. M. Anitas, M. Bunoiu, B. Vatzulik, I. Juganaru – J. Ind. Eng. Chem., **20**, 3994 (2014).
[15] J. A. Sotelo, V. N. Pustovit, G. A. Niklasson, Phys. Rev. B, **65**, 245113 (2002).
[16] B. Mandelbrot – "The Fractal Geometry of Nature", W. H. Freeman, USA, 1982.
[17] J. F. Gouyet – "Physics and Fractal Structures", Springer, Berlin, 1996.
[18] J. E. Martin and A. J. Hurd, J. Appl. Cryst. **20**, 61 (1987).
[19] J. Teixeira - J. Appl. Cryst. **21**, 781 (1988).
[20] D. H. Bale, P. W. Schmidt - Phys. Rev. Lett. **53**, 596 (1984).
[21] P. W. Schmidt and X. Dacai, Phys. Rev. A **33**, 560 (1986).
[22] P. W. Schmidt, J. Appl. Cryst. **24**, 414 (1991).
[23] A. Yu. Cherny, E. M. Anitas, A. I. Kuklin, M. Balasoiu, V. A. Osipov – J. Appl. Cryst. **43**, 790 (2010).
[24] A. Yu. Cherny, E. M. Anitas, A. I. Kuklin, M. Balasoiu, V. A. Osipov – J. Surf. Invest. X-ray Synchrotron and Neutron Techniques **4**, 903 (2010).
[25] A. Yu. Cherny, E. M. Anitas, V. A. Osipov, A. I. Kuklin – Phys. Rev. E **84**, 036203 (2011).
[26] A. Yu. Cherny, E. M. Anitas, V. A. Osipov, A. I. Kuklin – J. Appl. Cryst. **47**, 198 (2014).
[27] E. M. Anitas – Eur. Phys. J. B **87**, 139 (2014).
[28] G. Beaucage – J. Appl. Cryst. **28**, 717 (1995).

*Corresponding author: anitas@theor.jinr.ru